PCCP

RSC Publishing

PAPER

Integrated X-ray photoelectron spectroscopy and DFT characterization of benzene adsorption on Pt(111), Pt(355) and Pt(322) surfaces†

Cite this: *Phys. Chem. Chem. Phys.*, 2013, **15**, 20662

Renqin Zhang,‡[a] Alyssa J. Hensley,[a] Jean-Sabin McEwen,*[ab] Sandra Wickert,‡[c] Erik Darlatt,[c] Kristina Fischer,[c] Matthias Schöppke,[c] Reinhard Denecke,*[c] Regine Streber,[d] Michael Lorenz,[d] Christian Papp[d] and Hans-Peter Steinrück[d]

Received 24th July 2013,
Accepted 21st October 2013

DOI: 10.1039/c3cp53127a

www.rsc.org/pccp

We systematically investigate the adsorption of benzene on Pt(111), Pt(355) and Pt(322) surfaces by high-resolution X-ray photoelectron spectroscopy (XPS) and first-principle calculations based on density functional theory (DFT), including van der Waals corrections. By comparing the adsorption energies at 1/9, 1/16 and 1/25 ML on Pt(111), we find significant lateral interactions exist between the benzene molecules at 1/9 ML. The adsorption behavior on Pt(355) and Pt(322) is very different. While on Pt(355) a step species is clearly identified in the C 1s spectra at low coverages followed by occupation of a terrace species at high coverages, no evidence for a step species is found on Pt(322). These different adsorption sites are confirmed by extensive DFT calculations, where the most favorable adsorption configurations on Pt(355) and Pt(322) are also found to vary: a highly distorted across the step molecule is found on Pt(355) while a less distorted configuration adjacent to the step molecule is deduced for Pt(322). The theoretically proposed C 1s core level binding energy shifts between these most favorable configurations and the terrace species are found to correlate well with experiment: for Pt(355), two adsorbate states are found, separated by ~0.4 eV in XPS and 0.3 eV in the calculations, in contrast to only one state on Pt(322).

1. Introduction

Benzene is a simple yet important aromatic organic compound whose unique properties are central in much of modern chemistry. As a non-saturated hydrocarbon with a reactive π system, it chemisorbs on transition metal surfaces. The chemisorption of benzene on a catalyst surface is an important elementary step in many catalytic transformations, including its dehydrogenation and hydrogenation.[1–3] Furthermore, benzene can be the product of oxygen-removal reactions from aromatic compounds, such as phenol.[4] The understanding of the corresponding reaction pathways is of utmost importance for development of alternative renewable energy sources to replace our dwindling fossil fuel reserves.[5]

Platinum-based catalysts are widely studied and used in such reactions.[2,3,6–10] The adsorption of benzene on Pt(111) and Pt(110) surfaces has been studied by a number of experimental and computational methods in great detail.[11–20] Using calorimetric measurements, the adsorption energy of benzene on Pt(111) was found to decrease with increasing benzene coverage,[18] and from low-energy electron diffraction (LEED), a distortion of the benzene ring was deduced.[12] Such a distortion of the benzene molecule results in two important adsorption sites on Pt(111), namely, a bridge_30° and a hollow_0° site.[16,17]

Surface defects, such as steps,[8,21,22] reconstructions[14,23] and point defects[24] on single crystal surfaces, but also nanoparticles,[1] provide the active sites in many chemical reactions. This is attributed to a significantly changed atomic and electronic structure as compared to flat terraces. In that context, stepped surfaces are the more realistic catalytic surfaces. Steps can have a tremendous effect on the adsorption of molecules and their reaction pathways.[8,9,25] From a combined X-ray photoelectron spectroscopy (XPS) and density functional theory (DFT) study, Jacob *et al.* concluded that the oxidation of Pt(355) and Pt(322) surfaces occurs at step sites rather than terrace sites.[9] On Pt(355), step sites were clearly identified as the active sites for the oxidation of sulfur, which leads to a significantly enhanced activity of Pt(355) as compared to Pt(111).[8]

[a] *The Gene and Linda Voiland School of Chemical Engineering and Bioengineering, Washington State University, WA, 99164, USA. E-mail: js.mcewen@wsu.edu*
[b] *Department of Physics and Astronomy, Washington State University, WA, 99164, USA*
[c] *Wilhelm-Ostwald-Institut für Physikalische und Theoretische Chemie, Universität Leipzig, 04103 Leipzig, Germany. E-mail: denecke@uni-leipzig.de*
[d] *Lehrstuhl für Physikalische Chemie II, Friedrich-Alexander-Universität Erlangen-Nürnberg, 91054 Erlangen, Germany*

† Electronic supplementary information (ESI) available. See DOI: 10.1039/c3cp53127a

‡ Equivalent first authors.

Comparative studies of stepped surfaces with different step orientations, *e.g.*, Pt(355) and Pt(322), revealed differences for the steps of (111) and (100) orientation, respectively.[7,25,26] By *in situ* high-resolution XPS, it was demonstrated that the adsorption and desorption of CO on Pt(355) and Pt(322) behaved differently.[26,27] CO adsorbed at the steps on Pt(355) is more strongly bound than on the steps on Pt(322). Also, significant differences were observed in the step coverages of methyl and the characteristic dehydrogenation temperatures of methyl to methylidyne and subsequently to carbon on Pt(355) and Pt(322): both surfaces are more reactive than Pt(111), with Pt(355) showing a higher activity than Pt(322).[7,25] After studying these very simple adsorbates, it is important to expand the detailed investigation of the role of steps to more complex adsorption systems, *i.e.*, benzene on Pt(355) and Pt(322). Benzene is an ideal probe molecule to study surface properties because it is one of the most simple aromatic compounds and is highly symmetric.[16] Herein, we therefore present a systematical investigation of the adsorption of benzene on the stepped Pt(355) and Pt(322) surfaces, and for comparison also the flat Pt(111) surface. Our study combines *in situ* high-resolution XPS and first-principle calculations based on DFT, including van der Waals (vdW) interactions.

2. Experimental and computational methods

2.1 Experimental methods

All high-resolution XPS experiments were performed at the synchrotron facility, BESSY II, in Berlin (Germany) at beamline U49/2-PGM1 at Helmholtz Zentrum Berlin. A transportable UHV-station (background pressure below 5×10^{-10} mbar) was used, consisting of an analysis chamber and a preparation chamber, equipped with a LEED (low energy electron diffraction) optics, a quadrupole mass analyzer and a sputtering system. The electron energy analyzer was an OMICRON EA 125 U7 HR.[28]

Platinum single crystals with (111), (322) and (355) surface orientation were used. Pt(322) and Pt(355) both have five atom wide terraces, separated by monoatomic steps with (100) and (111) orientation, respectively, as shown in Fig. 1. The single crystals could be heated to 1200 K and cooled down to 90 K with a LN_2-cryostat. The temperature was measured by a K-type thermocouple spot-welded to the edge of the sample. For preparing a clean surface, the samples were sputtered with Ar ions and subsequently annealed to 1100 K. Carbon was removed by heating at 800 K in 5×10^{-7} mbar O_2. The clean surface was checked by LEED, verifying the step structure.[22] No contaminants could be detected by XPS.

The adsorption experiments were performed by dosing benzene (Merck, 99%; Emplura; purified by repeated pump–freeze–thaw cycles) onto the samples at 190 and 300 K using a capillary doser; at these temperatures no multilayer formation and no dissociation of benzene occurs. The benzene background pressure ranged for different experiments between 2×10^{-9} and 5×10^{-9} mbar, being enhanced at the sample by the capillary array doser. C 1s spectra were obtained with a photon energy of 380 eV with an overall resolution of 200 meV. Spectra were measured at normal emission (0°) or at 45° emission angle, and a typical measuring time of 8 s. In order to avoid radiation damage the measured spots on the surface were shifted by about 100 μm to a new spot for each step.

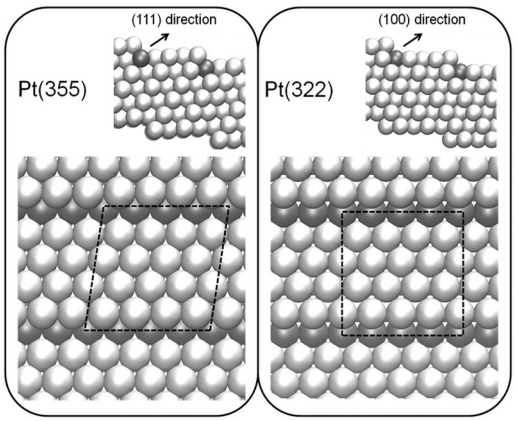

Fig. 1 Structure of the stepped Pt(355) and Pt(322) surfaces. The side view is shown in the smaller insets and the darker atoms emphasize the location of the step. Dashed lines represent the size of unit cells of Pt(355) and Pt(322) surfaces with the $p(4 \times 1)$ supercell we used in our calculations, which are (11.254 Å × 10.916 Å) and (11.254 Å × 11.621 Å), respectively.

The quantitative analysis of the XPS data was performed with peak fitting using UNIFIT.[29] In all C 1s spectra, the background and the curve fit were performed simultaneously. For the background a polynomial fit and a Shirley background was used. The C 1s curves were fitted with a Voigt function. Spectra were normalized to account for varying photon intensities. The binding energy scale was calibrated with respect to the Fermi energy.

2.2 Computational details

DFT calculations were performed with the Vienna *Ab initio* Simulation Package (VASP) code.[30,31] The projector augmented-wave (PAW)[32,33] method and the generalized-gradient approximation (GGA), using the PBE[34] functional, were employed for the treatment of the electron–ion interactions and the exchange–correlation effects, respectively. With its PAW potentials, VASP combines the accuracy of all-electron methods with the computational efficiency of plane-wave approaches. Electron dispersion interactions are known to play a crucial role in the properties of molecular adsorption on metal surfaces,[35–37] but their accurate description is highly challenging. While the random phase approximation (RPA) method has been proven to generate accurate surface and adsorption energies,[38] it still is computationally too demanding for the large size of the systems studied in this contribution. Therefore, the GGA-PBE functional was used with the inclusion of vdW corrections.[35]

The optB88-vdW functional was used as the exchange functional to account for vdW corrections.[35,36,39,40] For the ionic relaxation, the conjugate gradient algorithm was applied. The electronic wave functions were expanded in a basis set of plane waves with kinetic-energy cutoffs of 400 eV. The lattice constant of bulk Pt was calculated to be 3.986 Å, which is consistent with the literature result of 3.983 Å.[10] The stepped Pt(355) and

Pt(322) surfaces were modeled with $p(4 \times 1)$ supercells that were 6 layers thick (see Fig. 1), with the bottom 3 layers kept fixed in their bulk positions. The lattice dimensions of the Pt(355) and Pt(322) surfaces with the $p(4 \times 1)$ supercell are (11.254 Å × 10.916 Å) and (11.254 Å × 11.621 Å), respectively. They are nearly identical in size to the Pt(111) surface modeled with the $p(4 \times 4)$ supercell (11.254 Å × 11.254 Å). The thickness of the vacuum was approximately 15 Å. These unit cells were sampled with $(4 \times 4 \times 1)$ Monkhorst–Pack *k*-point grids. A Methfessel–Paxton smearing of 0.2 eV was used to improve the convergence and the total energy was extrapolated to zero Kelvin. The total energy convergence threshold was set to 10^{-5} eV and the geometries were considered to be fully relaxed when the forces were less than 0.015 eV Å^{-1}. In addition to the stepped surfaces, we also studied the Pt(111) surface for comparison. For this system, a 6 layers thick $p(4 \times 4)$ supercell was used with the bottom 4 layers kept fixed. The adsorption energy E_{ads} of benzene (C_6H_6) on each surface was calculated for different sites, and is defined as:

$$E_{ads} = E_{tot} - E_{slab} - E_{C_6H_6} \quad (1)$$

where E_{tot} is the total energy of C_6H_6/Pt, E_{slab} is the total energy of the clean Pt slab and $E_{C_6H_6}$ is the energy of a benzene molecule in the gas phase.

3. Results and discussion

3.1 Benzene on Pt(111)

We start with presenting results for benzene adsorption on the flat Pt(111) surface. This system serves as a reference for the two stepped surfaces. Fig. 2 shows a series of C 1s spectra collected during the dosing of benzene at 300 K (from bottom to top). At saturation (topmost spectrum) one peak at 284.5 eV is observed, with a shoulder at higher binding energy. This shoulder results from vibrational splitting due to excitation of the C–H-stretching mode in the photoionization process.[41,42] Fig. 3 (bottom trace) shows the fit of this vibrational fine structure, including the peaks due to the first and second excited state. The resulting vibrational splitting of 360 meV corresponds well to values found in XPS studies of other hydrocarbons.[42] With increasing coverage, a shift of the peak maximum of about 260 meV towards higher binding energies is observed in Fig. 2, which is attributed to lateral interactions between the benzene molecules.

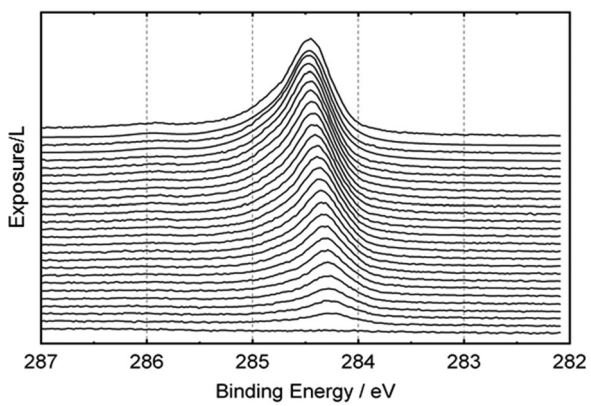

Fig. 2 C 1s spectra recorded during benzene uptake on Pt(111) at 300 K. The benzene exposure increases from bottom to top.

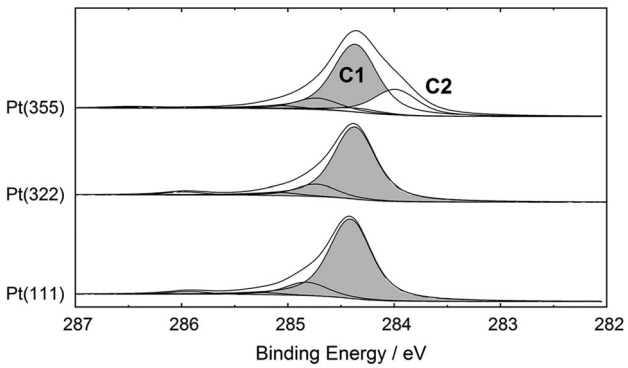

Fig. 3 Comparison between C 1s spectra for (bottom) Pt(111), (center) Pt(322) and (top) Pt(355), measured at saturation coverage of benzene following adsorption at 300 K. C1 (grey-shaded) and C2 mark the two distinct contributions on the Pt(355) surface.

The benzene coverage is calibrated by comparison to the XP spectra for CO on Pt(111).[43] For the saturated layer, a coverage of 1.1 C atoms per Pt atom is obtained, resulting in a benzene coverage of about 0.18 ML, which agrees with the result by Campbell *et al.*[11] An additional uptake experiment at 190 K (not shown) showed identical binding energies and peak shapes, as found for 300 K in Fig. 2, with the saturation coverage being larger by 3%.

The existence of only one single C 1s peak (with its vibrational satellite) indicates that all C atoms should be in a similar chemical state relative to the Pt surface atoms. In contrast, for benzene adsorption on Ni(111), a coverage-dependent shoulder was observed in the C 1s spectra.[42] This observation was assigned to a coverage-dependent change in the adsorption site, from a bridge-bonded geometry with two non-equivalent carbon atoms (yielding two C 1s peaks split by ~0.25 eV) to a hollow geometry with all six C atoms in an identical environment relative to Ni substrate (yielding only a single C 1s peak).[42] Following the arguments used for Ni(111), the single peak would indicate a similar environment for the six C atoms relative to the Pt surface atoms, and thus suggest a hollow adsorption site. The comparison to possible highly symmetric adsorption sites on Pt(111), depicted in Fig. 4, shows that this would be the case for the hcp_0°, fcc_0°, top_0° and top_30° configurations. However, these sites are in contrast to the literature, where the most favorable adsorption site of benzene on Pt(111) was found to be a bridge_30° site by theoretical calculations[16,17] and also by diffuse LEED.[12] One should mention here that for benzene on Pt(111), no well ordered superstructure could be observed, in agreement with literature,[12] but in contrast to Ni(111),[42] where a well-ordered $(\sqrt{7} \times \sqrt{7})R19.1^\circ$ structure was found.

In order to compare with the theoretical calculations by Sautet *et al.*,[17] we also calculated the adsorption energies of benzene on Pt(111) with a $p(3 \times 3)$ 4 layers slab. Different adsorption

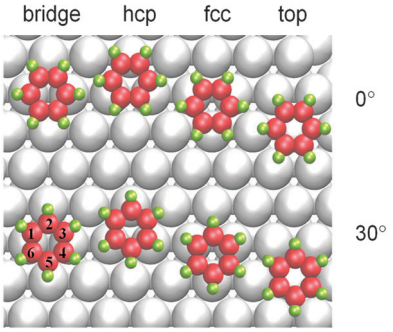

Fig. 4 Adsorption sites of benzene on Pt(111). The benzene C–C bonds can have rotations of 0° (upper panel) and 30° (lower panel) relative to the densely packed Pt rows. The biggest (grey), middle (red) and smallest (green) spheres represent Pt, C and H atoms, respectively. These notations and schemes are applied to the following figures as well.

Table 1 Adsorption energies of benzene on Pt(111), represented by a $p(4 \times 4)$ supercell and slab thickness of 6 layers. The results presented here include those calculations with (PBE + vdW) and without (PBE) vdW corrections. In order to compare with literature, results calculated on a Pt(111) surface with a $p(3 \times 3)$ unit cell and 4 layers are also listed. Values in parentheses are calculated with benzene constrained on these sites

	$p(3 \times 3)$_4 layers		$p(4 \times 4)$_6 layers	
Adsorption site	PBE	Sautet's results[a]	PBE	PBE + vdW
bridge_0°	−0.28	−0.30	−0.75	−1.58
bridge_30°	−0.89	−0.90	−1.36	−2.14
hcp_0°	−0.65	−0.67	−1.11	−1.89
hcp_30°	−0.25	−0.33	—[b]	(−1.27)[b]
fcc_0°	−0.58	−0.61	−1.04	−1.82
fcc_30°	−0.19	−0.27	—[b]	(−1.21)[b]
top_0°	—[b]	—[b]	0.04	−0.79
top_30°	—[b]	—[b]	—[b]	(−0.81)[b]

[a] This data is from ref. 17, where PW91 functional was used. [b] Unstable adsorption site.

sites of benzene on this surface are shown in Fig. 4. The results of the adsorption energies are listed in Table 1; they are in good agreement with those obtained previously (0.89 *vs.* 0.90 eV). As Sautet *et al.*[17] reported that slab thickness influences the adsorption energy, we also calculated benzene adsorbed on a bridge_30° site using $p(4 \times 4)$ 4 layers and $p(4 \times 4)$ 6 layers slabs. The adsorption energies were found to be −1.19 eV and −1.36 eV, respectively. Due to the significantly larger value for the thicker slab, we used the $p(4 \times 4)$ 6 layers slab to model the Pt(111) surface in our following calculations.

It has been reported that vdW corrections have a significant effect on calculated adsorption energies of benzene on transition metal surfaces.[35] We therefore performed calculations with vdW corrections for 6 layer slabs with $p(3 \times 3)$, $p(4 \times 4)$ and $p(5 \times 5)$ supercells, corresponding to coverages of 1/9, 1/16 and 1/25 ML. The adsorption energies of benzene on the bridge_30° site are −1.89 eV, −2.14 eV and −2.10 eV, respectively. Thus, the vdW corrections indeed lead to a pronounced increase of the adsorption energy for all calculated adsorption sites (see Table 1 for the $p(4 \times 4)$ 6 layers slab). The significant increase of the adsorption energy from the $p(3 \times 3)$ to the $p(4 \times 4)$ supercell indicates that the adsorbate coverage has a significant effect on the adsorption energy of benzene. From the lack of a significant difference between the $p(4 \times 4)$ and $p(5 \times 5)$ unit cells, we deduce that the lateral interaction between benzene molecules can be considered to be negligible already for the former unit cell. The calculated adsorption energies are consistent with the experimental results from microcalorimetry ranging between −2.04 eV at zero coverage to −1.81 eV at 1/9 ML.[18] They also agree well with previous computational results where an adsorption energy of −1.89 eV was obtained for the $p(3 \times 3)$ unit cell.[35]

As evident from Table 1, the addition of vdW corrections increases the adsorption energies of benzene on all sites, but the bridge_30° site remains the most stable site. Interestingly, the hcp_30° and fcc_30° sites became unstable when using the $p(4 \times 4)$ supercell and both shifted to the bridge_30° site. This implies that the lateral interactions between the molecules stabilize benzene on hcp_30° and fcc_30° sites in the $p(3 \times 3)$ supercell. To determine if these two sites have unfavorable adsorption energies, we calculated their adsorption energies with benzene constrained on these sites (optimize z direction only), which yielded values of −1.27 eV and −1.21 eV, respectively. While the negative values indicate that adsorption on these sites is thermodynamically favorable (if constrained), the observed shift to the more stable bridge_30° site indicates that there is no energy barrier for moving benzene between these sites. The comparison to the stable adsorption sites for the $p(3 \times 3)$ supercell in Table 1 shows that overall the order of the stability of the adsorption sites is unchanged, *i.e.* the fcc_30° site is the most unfavorable adsorption site with vdW corrections. The top_0° and top_30° sites are both unstable on the Pt(111) for the $p(3 \times 3)$ supercell, in agreement with Sautet *et al.*[17] When modeled within a $p(4 \times 4)$ supercell with vdW corrections the top_0° site is stable with an adsorption energy of −0.79 eV. The top_30° site remains unstable and shifts towards a bridge_30° site; when constraining the site we obtain a value of −0.81 eV.

3.2 Benzene on Pt(355)

In Fig. 5, the C 1s spectra taken during benzene adsorption at 300 K until saturation are shown. At low coverage, a single peak develops at ~284.0 eV (called C2). Around ~0.11 ML, this peak saturates and the growth of a second additional peak (C1) at ~284.4 sets in and continues to grow until saturation. In Fig. 3 (top) the spectrum of the saturated layer is fitted with these two contributions and their corresponding vibrational satellites. The C1 peak corresponds very well to the peak observed on Pt(111), and the C2 new peak is specific for the Pt(355) surface. The existence of two peaks indicates the existence of carbon atoms in a different chemical environment. At saturation, the intensity ratio of C1 to C2 is 3 : 1. An additional experiment at 190 K (not shown) yielded very similar results, with the C1 : C2 ratio at saturation being 4 : 1.

There are two possibilities for the observed two peak structure: either the two signals belong to one molecule with inequivalent C atoms (as was observed on Ni(111)[42]), or they are due to two

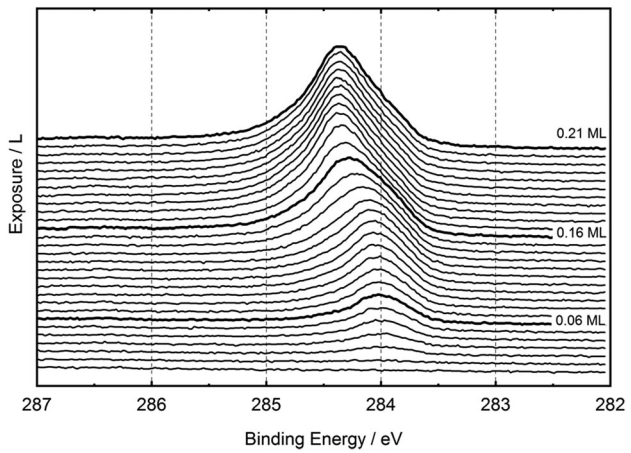

Fig. 5 C 1s spectra recorded during benzene uptake on Pt(355) at 300 K. On the right, benzene coverages, as derived from comparison to CO experiments, are displayed for the highlighted spectra. The top most spectrum is shown in more detail in Fig. 3.

molecules at different adsorption sites, *e.g.* on terraces and steps. Since for Pt(111) only one single peak was observed, we attribute the new peak (C2) to adsorption at the steps. This conclusion was proven by blocking the steps with one row of Ag (as already done in a previous study on CO adsorption[23]), and indeed the resulting uptake spectra only showed the C1 peak. Details of this experiment are reported elsewhere.[44] Consequently, C1 is assigned to benzene at terrace sites and C2 to benzene at step sites.

In the corresponding DFT calculations, which included vdW corrections, we first considered benzene adsorption on different Pt(355) terrace sites, as shown in Fig. 6, with the adsorption energies listed in Table 2. The corresponding results without vdW corrections again yielded much smaller values with differences between 0.6 and 0.9 eV (see Table S1 in ESI†). We need to point out that our conclusions are only based on low coverage

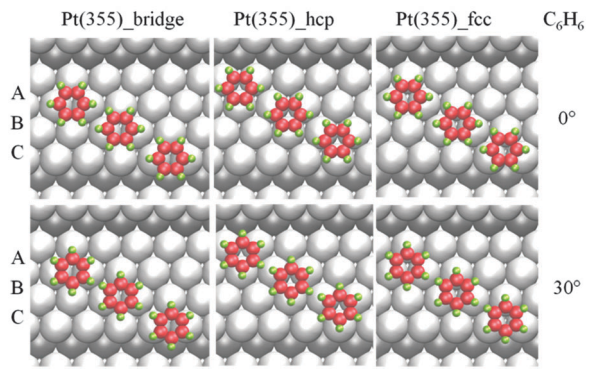

Fig. 6 Different adsorption sites of benzene on the terrace of the Pt(355) surface. These sites are similar to those seen on the Pt(111) surface, where benzene can adsorb on bridge, hcp and fcc sites. The labeled adsorption sites (A, B, C) denote a difference in the distance between benzene and the step row. Here, the C–C bonds in the benzene can have rotations of 0° (upper panel) and 30° (lower panel) with respect to the step row. Altogether, there are 18 adsorption sites considered on the terrace of Pt(355). Pt atoms in the step are presented by darker grey atoms.

Table 2 The adsorption energies (eV) of C_6H_6 at 1/16 ML on Pt(355) and Pt(322) surfaces. The results presented here were calculated by using PBE functional with vdW corrections. The results for the unstable adsorption of benzene on the hcp_30°, fcc_30° and bridgeC_0° sites are listed in Table 3

Adsorption sites	Pt(355)	Pt(322)
bridgeA_0°	−1.49	−1.56
bridgeB_0°	−1.42	−1.48
bridgeA_30°	−1.88	−1.97
bridgeB_30°	−1.87	−1.93
bridgeC_30°	−2.04	−2.12
hcpA_0°	−1.39	−1.69
hcpB_0°	−1.42	−1.62
hcpC_0°	−1.71	−2.40
fccA_0°	−1.45	−1.70
fccB_0°	−1.45	−1.55
fccC_0°	−2.14	−1.88
stepA_0°	−2.23[a]	−0.89
stepA_30°	−0.21	−2.16[a]
stepB_0°	−2.42	−1.80
stepB_30°	−2.23[a]	−1.98[a]

[a] Unstable site.

calculations (1/16 ML) and by considering one adsorption site at a time. We also note that, as mentioned in Section 2.2, that the size of unit cells used for Pt(355) and Pt(322) surfaces used here are nearly identical to that of the $p(4 \times 4)$ cell for the Pt(111) surface, so we believe that the unit cells used in this contribution are large enough to eliminate the benzene–benzene interaction on the Pt(355) and the Pt(322) surfaces.

We first discuss the A and B terrace type sites on the Pt(355) terrace, which are similar to those on Pt(111), where the most stable site is the bridge_30° site (−2.14 eV; see Table 1). Similarly, we find that among all the A and B sites, the bridgeA_30° site is the most favorable one with an adsorption energy of −1.88 eV; see Table 2. In addition, the fcc_0° and hcp_0° sites have nearly identical adsorption energies, similar to the situation for Pt(111). The difference of 0.45–0.49 eV between bridge_30° and hcp_0° sites on Pt(355) is larger than the value of 0.25 eV on Pt(111).

The adsorption energies on terrace C sites, *i.e.* close to the step, are higher than those of the A and B sites and therefore these sites are more favorable. For the bridgeC_30° site it is −2.04 eV, as compared to −1.88 eV and −1.87 eV for the bridgeA_30° and bridgeB_30° sites, respectively. This increase in adsorption energy is most likely due to the changed electronic structure at the steps. For the fccC_0° and hcpC_0° sites, we find a significant difference of ∼0.43 eV. Interestingly, the fccC_0° site is the most stable of all terrace sites on Pt(355) with an adsorption energy of −2.14 eV, which is even higher than the value of −2.04 eV for the bridgeC_30° site.

Fig. 7 depicts a number of possible step sites for benzene on Pt(355) (“across the step”): the top panel shows the starting (input) geometries for the calculations, and the bottom two panels are the final configurations. The corresponding adsorption energies as obtained from the calculation including vdW corrections are listed in Table 2. The results without vdW corrections are shown in Table S1 of ESI.† The adsorption

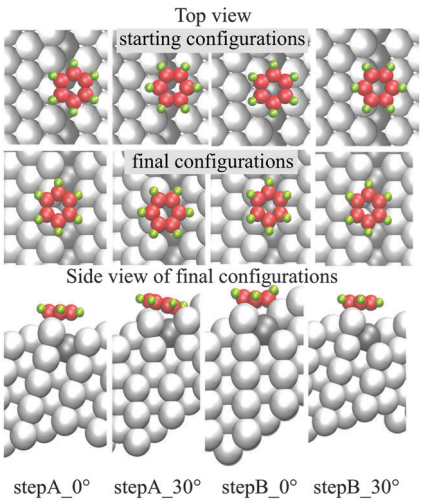

Fig. 7 The starting (top panel) and final configuration (bottom two panels with top and side views) of benzene on the step sites of Pt(355) surface.

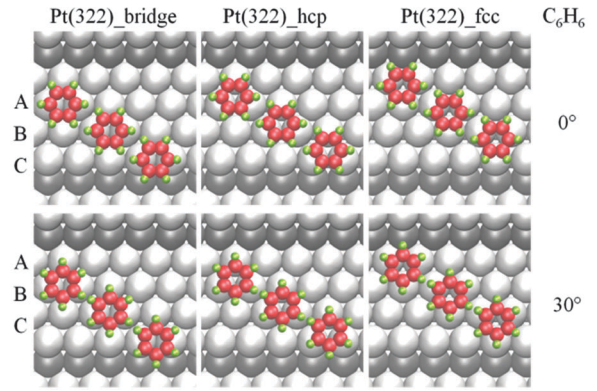

Fig. 8 Different adsorption sites of benzene on the terrace of the Pt(322) surface. These sites are similar to those seen on the Pt(111) surface, where benzene can adsorb on bridge, hcp and fcc sites. Each kind of adsorption site has three different positions relative to the step row and they are labeled as A, B, C. Here, the C–C bonds in the benzene can have rotations of 0° (upper panel) and 30° (lower panel) with respect to the step row. Thus, there are 18 adsorption sites on the terrace of Pt(322).

energies are typically smaller by ~0.8 eV and we note that the stepA_30° is only a stable site (−0.21 eV) with vdW corrections. The calculations show that benzene molecules at stepA_0° and stepB_30° sites are unstable and shift to a site similar to the bridgeC_0° site on the terrace (see Fig. 6), with a tilted geometry, and an adsorption energy of −2.23 eV. When comparing the adsorption of non-interacting benzene molecules on both terrace and step sites, it is clear that the most favorable adsorption site on the Pt(355) surface overall is the stepB_0° with an adsorption energy of −2.42 eV. This result explains the experimental observation of two benzene species on the Pt(355) surface, one at the steps, which due to its higher binding energy preferentially adsorbs at low coverages, and one at the terraces, which adsorbs only after the steps are saturated.

3.3 Benzene on Pt(322)

Benzene adsorption on Pt(322) at 300 K gives a similar result as on the flat Pt(111) surface. As evident from Fig. 3 (center), the peak shape and position at saturation are virtually identical. Similar to Pt(111), with increasing coverage a shift of the peak maximum by about 240 meV to higher binding energies is observed (data not shown). The saturation coverage on Pt(322) is only slightly lower than on Pt(111). Intuitively, one would have expected to observe a specific step species as observed for the Pt(355) surface (see above). Such a behavior was observed for, *e.g.*, CO on stepped Pt surfaces [22] and also for ethylene. However, in contrast to Pt(355), no obvious spectral difference can be observed during benzene uptake on Pt(322).

Complementary information is again obtained from DFT calculations including vdW corrections. Fig. 8 shows possible adsorption sites on the terrace of a Pt(322) surface, and the adsorption energies are listed in Table 2. The corresponding results without vdW corrections again yielded much smaller values with differences between 0.6 and 0.9 eV (see Table S1 in ESI†). As evident from Fig. 8, the A and B sites on the Pt(322) terraces are similar to those on the Pt(355) terrace and on Pt(111). As for Pt(355), among all A and B sites, the bridgeA_30° site is the most favorable site with an adsorption energy of −1.97 eV, and the adsorption energies on the fcc_0° and hcp_0° sites are nearly identical. The difference of 0.28–0.31 eV between the A and B bridge_30° and hcp_0° sites on Pt(322) is slightly larger than the value of 0.25 eV on Pt(111). This differs from the results for Pt(355), which showed a larger energy difference between the two terrace sites of 0.45–0.49 eV.

The C type sites, which are closer to the step, have more favorable adsorption energies than their terrace counterparts. For example, benzene on bridgeC_30° sites have an adsorption energy of −2.12 eV, as compared −1.97 and −1.93 eV for the bridgeA_30° and bridgeB_30° sites, respectively. Furthermore, the adsorption energies of the fcc_0° sites and hcp_0° sites differ by 0.52 eV, in contrast to the very similar values for the corresponding sites on the Pt(322) terrace and on Pt(111). Overall, the hcpC_0° site with an adsorption energy of −2.40 eV is the most stable site on the Pt(322) terrace, followed by the bridgeC_30° site with −2.12 eV.

In Fig. 9, a number of very specific possible benzene step sites on Pt(322) (''across the step'') are depicted: the top panel shows the starting (input) geometries for the calculations, and the bottom two panels are the final configurations. The corresponding adsorption energies as obtained from calculations including vdW corrections are listed in Table 2.

When comparing the starting configurations to the optimized geometries, it is evident that the stepA_30° and stepB_30° configurations are unstable: while their initial configurations had their benzene rings parallel to the [100] step, their final configurations have the benzene rings almost parallel to the (111) terrace, with adsorption energies of −2.16 eV and −1.98 eV, respectively. The adsorption energies on the stepA_0° site (−0.89 eV) and on the stepB_0° site (−1.80 eV) are lower than on the hcpC_0° terrace site (−2.40 eV), which overall is the most favorable adsorption site on Pt(322). Therefore, benzene does not prefer to adsorb onto the ''across the step'' sites on Pt(322),

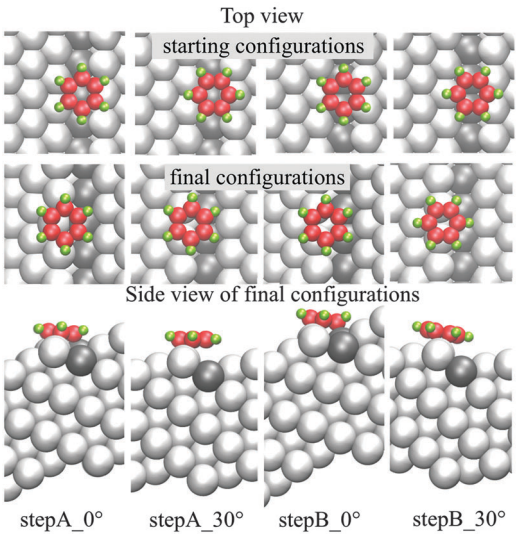

Fig. 9 The starting (top panel) and final configuration (bottom two panels with top and side views) of benzene on the step sites of the Pt(322) surface.

in contrast to Pt(355). This behavior explains, why only one benzene species was observed by high-resolution XPS in Fig. 3.

3.4 "Unstable" terrace sites on Pt(355) and Pt(322)

For adsorption of benzene on both Pt(355) and Pt(322), all hcp_30° and fcc_30° terrace sites were found to be unstable in the DFT calculations; this is illustrated in Fig. 10. In Table 3, the corresponding adsorption energies of the starting configurations, as calculated by constraining the molecule to this site (fix the x and y direction, relax z direction only) and of the shifted sites are summarized. Note that in all cases, the adsorption energy of benzene at the constrained site is negative, meaning that the adsorption on these sites (if constrained) is thermodynamically favorable. From the fact that benzene shifted to a more stable site, we conclude that there is no energy barrier between these adsorption sites.

For Pt(355), benzene shifted from the (starting) hcpB_30° site (−1.02 eV) and hcpC_30° sites (−1.09 eV) to the bridgeB_30° adsorption site (−1.87 eV; see Table 3). Similarly, benzene on hcpA_30° and fccA_30° sites shifted to bridge_30° site with an adsorption energy of −1.73 eV (note that this site has a different distance to the step edge than the other bridge_30° sites in Fig. 6). Benzene on the fccB_30° and fccC_30° sites shifted to a bridge_30° and the bridgeC_30° sites, respectively, with adsorption energies of −1.70 and −2.04 eV, respectively.

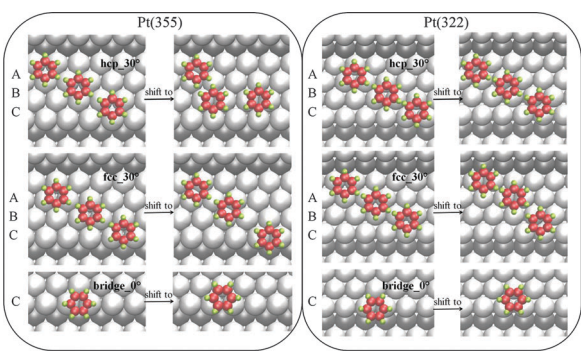

Fig. 10 Unstable adsorption sites and the corresponding shifted sites of benzene on the terrace of the Pt(355) and Pt(322) surfaces.

Table 3 The comparison of the adsorption energy of benzene kept on the unstable adsorption sites with that on shifted sites for Pt(355) and Pt(322) surfaces, as shown in Fig. 10. All values were calculated with the inclusion of vdW corrections

	Pt(355)		Pt(322)	
Adsorption sites	Fix_xy	Shifted site	Fix_xy	Shifted site
hcpA_30°	−0.96	−1.73	−1.23	−1.99
hcpB_30°	−1.02	−1.87	−1.09	−1.85
hcpC_30°	−1.09	−1.87	−1.56	−2.34
fccA_30°	−1.05	−1.73	−1.12	−1.80
fccB_30°	−0.98	−1.70	−1.02	−1.97
fccC_30°	−1.34	−2.04	−1.23	−2.35
bridgeC_0°	−1.88	−2.14	−1.99	−2.40

For Pt(322), benzene initially placed on any of the fcc_30° sites moves to more favorable bridge_30° sites, as shown in Fig. 10, *i.e.* from the fccB_30° sites to bridgeA_30° with adsorption energies of −1.97 eV. Moreover, benzene on the fccA_30° and fccC_30° sites shift to bridge_30° sites with adsorption energies of −1.80 and −2.35 eV, respectively (see Table 3). Similar shifts are obtained for benzene on hcp_30° sites.

3.5 C 1s core-level binding energy shifts in adsorbed benzene

The core-level binding energy is defined as the energy to remove a core electron from an atom, and can serve as a bridge to connect experimental and computational results.[42,45] Papp *et al.* used X-ray photoelectron spectroscopy, combined with the available information on molecular orientation, to verify the adsorption site of benzene on Ni(111).[42] To correlate the DFT calculations with our experimental results in Fig. 3, we calculated the core level binding energy shifts between the various adsorption configurations using the so-called final state approximation.[45] The calculated shifts can be used to identify the preferential adsorption site of benzene on our model surfaces.

In Section 3.1, lateral interactions were made responsible for the increase in the C 1s core-level binding energy with increasing benzene coverage on Pt(111). This effect of the lateral interactions for different coverages can be recovered theoretically by examining the core level binding energies for the bridge_30° configuration shown in Fig. 1. By using the C 1s binding energy on a $p(5 \times 5)$ unit cell as a reference, we find that the C 1s core-level for the $p(4 \times 4)$ and $p(3 \times 3)$ supercells are shifted by 0.04 and 0.15 eV, respectively, which is in qualitative agreement with experiment, where a shift of 0.26 eV was observed.

Next, we examine the resulting core level binding energy shifts of the different carbon atoms within benzene ring on the Pt(111), Pt(322) and Pt(355) surfaces. Based on our calculations above, the most stable benzene adsorption sites are the bridge_30° site on Pt(111), the hcpC_0° site on Pt(322), and the stepB_0° site on Pt(355). Note that among all possible adsorption sites of benzene on a Pt(355) surface, the stepB_0°

site was the most favorable. Although the difference of adsorption energy between benzene at the fccC_0° and stepB_0° sites is 0.28 eV, which is small, benzene will first adsorb on the stepB_0° site at low coverage. The maximum differences between carbon atoms within the benzene ring are calculated to be 0.12, 0.11, and 0.23 eV for Pt(111), Pt(322) and Pt(355) surfaces, respectively. On the other hand, the respective maximum differences for the terrace bridgeA_30° sites on Pt(355) and Pt(322) are 0.13 eV and 0.15 eV. These results are consistent with the experimental result that narrow C 1s peaks are observed on Pt(111) and Pt(322) in Fig. 3. In comparison, the core level binding energy shift is about 0.25 eV between carbon atoms within the ring of benzene adsorbed on a bridge_30° site of a Ni(111) surface.[42] This compares well with the calculated shift of 0.25 eV for Ni(111)[46] and is significantly smaller than the value of 0.12 eV for Pt(111). This explains why no measurable shift was detected for benzene on Pt(111): it is too small to be detected experimentally. The larger calculated value of 0.23 eV for Pt(355) is difficult to identify in Fig. 3 due to the overlapping signal of the terrace and step sites.

For the further analysis, we computed the C 1s core level shifts for the step sites relative to the most favorable terrace sites on Pt(355) and Pt(322). The E_{CLS} was defined as:

$$E_{CLS}(i) = E_{CL}(\text{bridge\_30\_C1}) - E_{CL}(\text{C\_}i) \qquad (2)$$

where E_{CL}(bridge_30_C1) is the core level energy of carbon atom 1 for benzene on a terrace bridge_30° site on Pt(322) or Pt(355), as shown in Fig. 11a. E_{CL}(C_i) is the core level energy of carbon atom i for benzene in its most favorable site, *i.e.* stepB_0° on Pt(355) and hcpC_0° on Pt(322), as shown in Fig. 11b. Note that the core level binding energy differences between the carbon atoms in benzene on the terrace bridge_30° sites are small on Pt(322) and Pt(355) (see Table S3 in ESI†) and these variations do not affect the conclusions below.

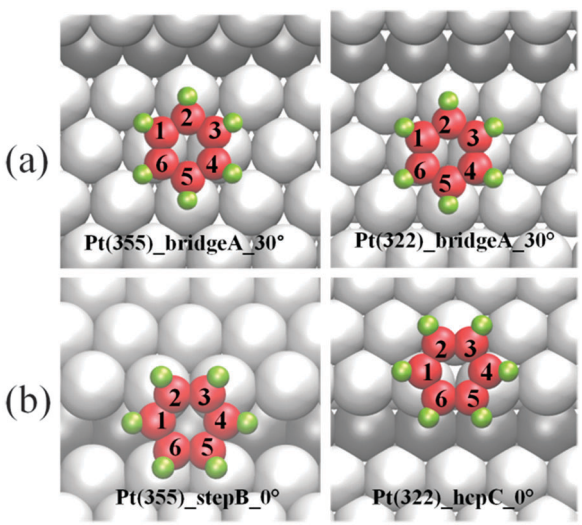

Fig. 11 Numbered carbons in benzene adsorbed on (a) the most favorable adsorption site on the terrace of Pt(355) and Pt(322), (b) the most favorable adsorption sites of Pt(355)_stepB_0°, Pt(322) _hcpC_0°.

Table 4 Core level binding energy shifts (E_{CLS} in unit of eV) of C 1s in benzene on the most stable adsorption sites for Pt(355) and Pt(322) surfaces relative to the most stable terrace bridge_30° site. The associated numbered carbons are shown in Fig. 11. These results are calculated by considering vdW corrections

Carbon	Pt(355)	Pt(322)
1	0.31	0.06
2	0.18	0.03
3	0.18	0.03
4	0.33	0.06
5	0.41	0.14
6	0.40	0.14

The resulting E_{CLS} for Pt(355) and Pt(322) are shown in Table 4, as calculated with vdW corrections; the shifts were found to be independent of the vdW corrections (see Table S2 in ESI†). The E_{CLS} for Pt(355) yields values from 0.18 to 0.41 eV, with an average value of 0.30 eV. Within the uncertainty of the calculations, this is consistent with the experimentally observed binding energy peak difference of about ~0.4 eV for the terrace and step species on Pt(355) (see shift between C1 and C2 component in Fig. 3). We should note that we take the convention that the core level binding energies are positive here. As a result, the core level binding energies shift to smaller values when adsorbed at the step sites on the Pt(355) surface, in agreement between experiment and theory.

For the Pt(322) surface, we observe only much smaller core level shifts of 0.03 to 0.14 eV (Table 4), with an average of 0.08 eV relative to the bridge_30° terrace site. Again, this is consistent with our XPS results, where we observe only one species with no sign of a core level shifted step species within the given experimental resolution.

3.6 Internal structure of benzene on Pt(111), Pt(355) and Pt(322)

It is reported that benzene adsorption on metals results in the H atoms being tilted away from the surface.[22,47,48] Therefore, as additional information, we calculated the geometric structure of benzene in the most stable adsorption sites on Pt(111), Pt(355) and Pt(322). Table 5 lists the corresponding information, as well as gas phase data. Overall, the C–C bond length in adsorbed benzene is increased relative to the free molecule, due to adsorbate–substrate interaction with a net electron transfer from benzene to the substrate. The H atoms tilt away from the surface to form an angle with the plane of the benzene ring, as it was found for benzene on various metal surfaces.[47]

The most favorable adsorption site for benzene on Pt(111) is the bridge_30° site, as shown in Fig. 1, where the carbon atoms 1, 3, 4 and 6 are equivalent, as well as carbon atoms 2 and 5. This leads to two different C–C bond lengths of about 1.432 and 1.474 Å, which is consistent with the literature.[17] In addition, despite negligible changes of the C–H bond lengths from 1.092 Å for free benzene to 1.099 Å and 1.094 Å, the H atoms tilt with dihedral angles of 18° and 35°.

The situation becomes more complex on Pt(355) and Pt(322). The most favorable adsorption configurations are the stepB_0° and hcpC_0° sites are shown in Fig. 11, respectively.

Table 5 The bond length of C–C bond C_{ij} in benzene (adsorbed the most favorable site) and the dihedral angle (θ_{H-C}) of the H atom away from the plane of benzene ring. The numbered carbon atoms are shown in Fig. 4 and 11. θ_{H-C} is defined as the angle between H–C bond and benzene ring. *Because some carbon atoms are in the same chemical environment, we just list θ_{H-C} value for one of them*

Benzene	C_{12} (Å)	C_{23} (Å)	C_{34} (Å)	C_{45} (Å)	C_{56} (Å)	C_{61} (Å)	θ_{H-C1}	θ_{H-C2}	θ_{H-C5}	Adsorption site
Free	1.398	1.398	1.398	1.398	1.398	1.398	0°	0°	0°	—
Pt(111)	1.473	1.472	1.432	1.474	1.474	1.433	18°	35°	35°	bridge_30°
Pt(355)	1.435	1.466	1.435	1.488	1.505	1.488	16°	22°	51°	stepB_0°
Pt(322)	1.468	1.426	1.467	1.436	1.458	1.436	22°	17°	17°	hcpC_0°

In this configuration, carbon 1 and 4 are equivalent, as well as carbon 2 and 3 and carbon 5 and 6. On Pt(355), C_{56} is the longest bond with 1.505 Å, which is 0.107 Å longer than in the free benzene molecule. The largest tilt angle θ_{H-C} of 51° is observed for H atoms bonded to carbon 5 and 6, which correlates well with the largest core level shifts for these atoms (Table 4). On Pt(322), the differences among all benzene C–C bond lengths are small, where the largest value of 0.042 Å being the difference between C_{12} and C_{23} (see Table 5). Although the tilt angles, θ_{H-C}, for Pt(322) are 17° and 22°, which is significantly different from that found on Pt(111), the core-level shift for Pt(322) does not change much as we move from carbon to carbon within the aromatic ring. As a result, the tilt angle is more sensitive to such configurational changes than the core level binding energy shift.

Since the most pronounced changes are observed for the stepB_0° adsorption site on Pt(355), we discuss this case in more detail. As evident from Fig. 7, the geometry of the adsorbed benzene molecule is strongly distorted due to its interaction with the surface. The C–H bonds form dihedral angles of 16°, 22° and 51°, with respect to the planar benzene ring. While there is no report on benzene adsorption on Pt(355), a distorted adsorption geometry has been reported for benzene on the reconstructed and highly corrugated $p(1 \times 2)$ Pt(110) surface from NEXAFS and angle-resolved UPS.[14] The experimental results suggested two forms of benzene on this surface: a highly distorted low-coverage form, and an essentially undistorted high-coverage form.[13,15,49] As our calculations of benzene Pt(355) mimics the low coverage situation, the observed strong distortion is in line with low-coverage configuration on the $p(1 \times 2)$ Pt(110) surface.

4. Conclusion

In summary, the adsorption of benzene on stepped Pt(355) and Pt(322) surfaces was systematically investigated by high-resolution X-ray photoelectron spectroscopy and first-principles calculations based on density functional theory including vdW corrections. Experimentally, it was found that the most favorable adsorption sites of benzene are different for the Pt(355) and Pt(322) surfaces, as seen by different C 1s binding energies and a clear development of step species on Pt(355). The DFT calculations also yielded different most favorable sites, which were the stepB_0° and hcpC_0° sites on Pt(355) and Pt(322), respectively. The step atoms affect on the adsorption behavior of benzene on terrace sites close to the step. We also demonstrated that the vdW corrections qualitatively change the adsorption energies of benzene on Pt surfaces. However, the core-level binding energy shift of the C 1s level in adsorbed benzene is independent of the chosen vdW corrections. The theoretically proposed core level binding energy shifts corroborate the differences found in the C 1s spectra of benzene on Pt(355) and Pt(322) surfaces. These differences result from the occurrence of two different benzene adsorption sites on Pt(355), benzene on a terrace site and adsorbed across the step site which produces a significant change in the core level binding energy.

Acknowledgements

This work was supported by institutional funds provided to JSM from the Voiland School of Chemical Engineering and Bioengineering. JSM would also like to thank Prof. Pierre Gaspard and Prof. William F. Schneider for their encouragement during the initial stages of this work. Experimental work at BESSY II was supported by BMBF (05 ES3XBA/5). We would also like to thank the staff at BESSY II for their support during beamtimes. We thank HZB for the allocation of synchrotron radiation beamtime. HPS and CP would like to gratefully acknowledge funding by the Cluster of Excellence 'Engineering of Advanced Materials' (www.eam.uni-erlangen.de) at the Universität Erlangen-Nürnberg.

References

1 K. M. Bratlie, H. Lee, K. Komvopoulos, P. Yang and G. A. Somorjai, *Nano Lett.*, 2007, **7**, 3097–3101.
2 W. Gao, W. T. Zheng and Q. Jiang, *J. Chem. Phys.*, 2008, **129**, 164705–164708.
3 C. Morin, D. Simon and P. Sautet, *Surf. Sci.*, 2006, **600**, 1339–1350.
4 A. Hensley, R. Zhang, Y. Wang and J.-S. McEwen, *unpublished work*, 2013.
5 J. Sun, A. M. Karim, H. Zhang, L. Kovarik, X. Li, A. J. Hensley, J.-S. McEwen and Y. Wang, *J. Catal.*, 2013, **306**, 47–57.
6 W. Yu, M. D. Porosoff and J. G. Chen, *Chem. Rev.*, 2012, **112**, 5780–5817.
7 C. Papp, T. Fuhrmann, B. Tränkenschuh, R. Denecke and H. P. Steinrück, *Chem. Phys. Lett.*, 2007, **442**, 176–181.
8 R. Streber, C. Papp, M. P. A. Lorenz, A. Bayer, R. Denecke and H.-P. Steinrück, *Angew. Chem., Int. Ed.*, 2009, **48**, 9743–9746.
9 J. Bandlow, P. Kaghazchi, T. Jacob, C. Papp, B. Tränkenschuh, R. Streber, M. P. A. Lorenz, T. Fuhrmann, R. Denecke and H. P. Steinrück, *Phys. Rev. B: Condens. Matter Mater. Phys.*, 2011, **83**, 174107.

10 J. S. McEwen, J. M. Bray, C. Wu and W. F. Schneider, *Phys. Chem. Chem. Phys.*, 2012, **14**, 16677–16685.
11 J. M. Campbell, S. Seimanides and C. T. Campbell, *J. Phys. Chem.*, 1989, **93**, 815–826.
12 A. Wander, G. Held, R. Q. Hwang, G. S. Blackman, M. L. Xu, P. de Andres, M. A. Van Hove and G. A. Somorjai, *Surf. Sci.*, 1991, **249**, 21–34.
13 N. C. Chen, L. P. Ford and R. I. Masel, *Catal. Lett.*, 1998, **56**, 105–109.
14 P. Zebisch, M. Stichler, P. Trischberger, M. Weinelt and H. P. Steinrück, *Surf. Sci.*, 1998, **396**, 61–77.
15 F. S. Thomas, N. S. Chen, L. P. Ford and R. I. Masel, *Surf. Sci.*, 2001, **486**, 1–8.
16 M. Saeys, M.-F. Reyniers, G. B. Marin and M. Neurock, *J. Phys. Chem. B*, 2002, **106**, 7489–7498.
17 C. Morin, D. Simon and P. Sautet, *J. Phys. Chem. B*, 2003, **107**, 2995–3002.
18 H. Ihm, H. M. Ajo, J. M. Gottfried, P. Bera and C. T. Campbell, *J. Phys. Chem. B*, 2004, **108**, 14627–14633.
19 C. Morin, D. Simon and P. Sautet, *J. Phys. Chem. B*, 2004, **108**, 5653–5665.
20 M. K. Sabbe, L. Lain, M.-F. Reyniers and G. B. Marin, *Phys. Chem. Chem. Phys.*, 2013, **15**, 12197–12214.
21 M. L. Honkela, J. Bjork and M. Persson, *Phys. Chem. Chem. Phys.*, 2012, **14**, 5849–5854.
22 L. Delle Site and D. Sebastiani, *Phys. Rev. B: Condens. Matter Mater. Phys.*, 2004, **70**, 115401.
23 T. Zhu, S.-G. Sun, R. A. van Santen and E. J. M. Hensen, *J. Phys. Chem. C*, 2013, **117**, 11251–11257.
24 B. Poelsema, K. Lenz and G. Comsa, *J. Chem. Phys.*, 2011, **134**, 074703–074710.
25 C. Papp, B. Tränkenschuh, R. Streber, T. Fuhrmann, R. Denecke and H. P. Steinrück, *J. Phys. Chem. C*, 2007, **111**, 2177–2184.
26 B. Tränkenschuh, C. Papp, T. Fuhrmann, R. Denecke and H. P. Steinrück, *Surf. Sci.*, 2007, **601**, 1108–1117.
27 R. Streber, B. Trankenschuh, J. Schock, C. Papp, H. P. Steinruck, J. S. McEwen, P. Gaspard and R. Denecke, *J. Chem. Phys.*, 2009, **131**, 064702–064709.
28 R. Denecke, M. Kinne, C. M. Whelan and H.-P. Steinrück, *Surf. Rev. Lett.*, 2002, **09**, 797–801.
29 R. Hesse and R. Denecke, *Surf. Interface Anal.*, 2011, **43**, 1514–1526.
30 G. Kresse and J. Furthmüller, *Phys. Rev. B: Condens. Matter Mater. Phys.*, 1996, **54**, 11169.
31 G. Kresse and J. Hafner, *Phys. Rev. B: Condens. Matter Mater. Phys.*, 1993, **47**, 558.
32 P. E. Blöchl, *Phys. Rev. B: Condens. Matter Mater. Phys.*, 1994, **50**, 17953.
33 G. Kresse and D. Joubert, *Phys. Rev. B: Condens. Matter Mater. Phys.*, 1999, **59**, 1758–1775.
34 J. P. Perdew, K. Burke and M. Ernzerhof, *Phys. Rev. Lett.*, 1996, **77**, 3865.
35 W. Liu, J. Carrasco, B. Santra, A. Michaelides, M. Scheffler and A. Tkatchenko, *Phys. Rev. B: Condens. Matter Mater. Phys.*, 2012, **86**, 245405.
36 J. Klimes and A. Michaelides, *J. Chem. Phys.*, 2012, **137**, 120901–120912.
37 R. Peköz, K. Johnston and D. Donadio, *J. Phys. Chem. C*, 2012, **116**, 20409–20416.
38 L. Schimka, J. Harl, A. Stroppa, A. Grüneis, M. Marsman, F. Mittendorfer and G. Kresse, *Nat. Mater.*, 2010, **9**, 741–744.
39 J. Klimeš, D. R. Bowler and A. Michaelides, *Phys. Rev. B: Condens. Matter Mater. Phys.*, 2011, **83**, 195131.
40 W. Liu, V. G. Ruiz, G.-X. Zhang, B. Santra, X. Ren, M. Scheffler and A. Tkatchenko, *New J. Phys.*, 2013, **15**, 053046.
41 H.-P. Steinrück, T. Fuhrmann, C. Papp, B. Tränkenschuh and R. Denecke, *J. Chem. Phys.*, 2006, **125**, 204706.
42 C. Papp, T. Fuhrmann, B. Tränkenschuh, R. Denecke and H. P. Steinrück, *Phys. Rev. B: Condens. Matter Mater. Phys.*, 2006, **73**, 235426.
43 M. Kinne, T. Fuhrmann, C. M. Whelan, J. F. Zhu, J. Pantförder, M. Probst, G. Held, R. Denecke and H.-P. Steinrück, *J. Chem. Phys.*, 2002, **117**, 10852.
44 S. Wickert, PhD thesis, Universität Leipzig, 2013.
45 L. Köhler and G. Kresse, *Phys. Rev. B: Condens. Matter Mater. Phys.*, 2004, **70**, 165405.
46 R. Zhang and J.-S. McEwen, unpublished result.
47 S. J. Jenkins, *Proc. R. Soc. A*, 2009, **465**, 2949–2976.
48 F. Mittendorfer and J. Hafner, *Surf. Sci.*, 2001, **472**, 133–153.
49 F. Thomas, N. Chen, I. Lee, L. Ford, P. Blowers and R. I. Masel, *J. Vac. Sci. Technol., A*, 1999, **17**, 2339–2344.